Monthly Notices of the ROYAL ASTRONOMICAL SOCIETY

MNRAS **535,** 2939–2947 (2024) https://doi.org/10.1093/mnras/stae2434
Advance Access publication 2024 October 28

Spectroscopic analysis of the strongly lensed SN Encore: constraints on cosmic evolution of Type Ia supernovae

S. Dhawan [1★] J. D. R. Pierel,[2†] M. Gu,[3] A. B. Newman,[4] C. Larison,[5] M. Siebert,[2] T. Petrushevska,[6] F. Poidevin,[7,8] S. W. Jha [5] W. Chen,[9] Richard S. Ellis,[10] B. Frye,[11] J. Hjorth,[12] Anton M. Koekemoer [2] I. Pérez-Fournon,[7,8] A. Rest,[2,13] T. Treu [14] R. A. Windhorst[15] and Y. Zenati[2,13]

[1]*Institute of Astronomy and Kavli Institute for Cosmology, University of Cambridge, Madingley Road, Cambridge CB3 0HA, UK*
[2]*Space Telescope Science Institute, Baltimore, MD 21218, USA*
[3]*Department of Physics, The University of Hong Kong, Pok Fu Lam 999077, Hong Kong*
[4]*Observatories of the Carnegie Institution for Science, 813 Santa Barbara St, Pasadena, CA 91101, USA*
[5]*Department of Physics & Astronomy, Rutgers, State University of New Jersey, 136 Frelinghuysen Road, Piscataway, NJ 08854, USA*
[6]*University of Nova Gorica, Center for Astrophysics and Cosmology, Vipavska 11c, SI-5270 Ajdovščina, Slovenia*
[7]*Instituto de Astrofísica de Canarias, Vía Láctea, E-38205 La Laguna, Tenerife, Spain*
[8]*Departamento de Astrofísica, Universidad de La Laguna, E-38206 La Laguna, Tenerife, Spain*
[9]*Department of Physics, Oklahoma State University, 145 Physical Sciences Bldg, Stillwater, OK 74078, USA*
[10]*Department of Physics & Astronomy, University College London, London WC1E 6BT, UK*
[11]*Department of Astronomy/Steward Observatory, University of Arizona, 933 Cherry Avenue, Tucson, AZ 85721, USA*
[12]*DARK, Niels Bohr Institute, University of Copenhagen, Jagtvej 155A, DK-2200 Copenhagen, Denmark*
[13]*Physics and Astronomy Department, Johns Hopkins University, Baltimore, MD 21218, USA*
[14]*Physics and Astronomy Department, University of California, Los Angeles, CA 90095, USA*
[15]*School of Earth and Space Exploration, Arizona State University, Tempe, AZ 85287-1404, USA*

Accepted 2024 October 17. Received 2024 October 17; in original form 2024 July 23

ABSTRACT

Strong gravitational lensing magnifies the light from a background source, allowing us to study these sources in detail. Here, we study the spectra of a $z = 1.95$ lensed Type Ia supernova (SN Ia) SN Encore for its brightest image A, taken 39 d apart. We infer the spectral age with template matching using the supernova identification (SNID) software and find the spectra to be at 29.0 ± 5.0 and 37.4 ± 2.8 rest-frame days post-maximum, respectively, consistent with separation in the observer frame after accounting for time dilation. Since SNe Ia measure dark energy properties by providing relative distances between low- and high-z SNe, it is important to test for the evolution of spectroscopic properties. Comparing the spectra to composite low-z SN Ia spectra, we find strong evidence of the similarity between the local sample and SN Encore. The line velocities of common SN Ia spectral lines, Si II 6355 Å and Ca II near-infrared triplet, are consistent with the distribution for the low-z sample as well as other lensed SNe Ia, e.g. iPTF16geu ($z = 0.409$) and SN H0pe ($z = 1.78$). The consistency between the low-z sample and lensed SNe at high-z suggests no obvious cosmic evolution demonstrating their use as high-z distance indicators, though this needs to be confirmed/refuted via a larger sample. We also find that the spectra of SN Encore match the predictions for explosion models very well. With future large samples of lensed SNe Ia, e.g. with the Vera C. Rubin Observatory, spectra at such late phases will be important to distinguish between different explosion scenarios.

Key words: supernovae: general – supernovae: individual: SN Encore.

1 INTRODUCTION

Type Ia supernovae (SNe Ia) are thermonuclear explosions of carbon–oxygen (CO) white dwarfs (WDs) in a binary system (see Maguire 2017; Livio & Mazzali 2018; Jha, Maguire & Sullivan 2019, for a review of the likely progenitor systems and observational properties of SNe Ia). Their bright peak luminosity and largely uniform observable characteristics across the population make them excellent distance indicators. SNe Ia have been instrumental in the discovery of accelerated expansion (Riess et al. 1998; Perlmutter et al. 1999) and for precision estimates of dark energy properties (Brout et al. 2022; DES Collaboration 2024; DESI Collaboration 2024) as well as the present-day expansion rate, i.e. the Hubble constant (Riess et al. 2022). In optical wavelengths, the regime where most constraints on cosmology from SNe Ia are obtained, standardization of their peak luminosity can reduce the scatter to ∼15 per cent. To obtain such a small scatter, the peak brightness is corrected for correlations with the light-curve width and colour (e.g. Phillips 1993; Tripp 1998) and also the host galaxy properties (e.g. Kelly et al. 2010; Sullivan et al. 2010; Ginolin et al. 2024a,b).

★ E-mail: sd919@cam.ac.uk, suhail.dhawan@gmail.com
† NASA Einstein Fellow.

Measuring dark energy properties with SNe Ia requires relative distance measurements, comparing the stretch and colour-corrected brightness of the high-z SNe Ia with a low-z 'anchor' sample (e.g. Brout et al. 2022; DES Collaboration 2024). Near-future experiments to study dark energy will sizably increase the sample of SNe Ia at very high-z, i.e. $z \gtrsim 2$ (Hounsell et al. 2018). With such large samples, the SN Ia constraints on dark energy will be dominated by systematic uncertainties. One possible significant source of error is the evolution of the progenitor population of SNe Ia with redshift. Studies of the SN Ia properties and their host galaxies suggest that it is likely that SNe Ia arise from more than one progenitor channel (e.g. Scalzo, Ruiter & Sim 2014; Childress et al. 2015; Dhawan et al. 2018; Maguire et al. 2018; Flörs et al. 2020, amongst others). It is, therefore, also possible that the relative fraction of the different channels giving rise to SNe Ia is not the same in the local and high-z universe leading to a redshift evolution of the SN Ia brightness, which cannot be corrected by the current standardization process. This would limit our ability to disentangle this evolution from differences in dark energy properties (e.g. Riess & Livio 2006).

Strong gravitational lensing is a novel window to studying high-z SNe. The 'gravitational telescope' effect (Zwicky 1937) magnifies the light from distant sources, allowing us to study the systems in detail. Spectra of gravitationally lensed SNe (gLSNe) have been used to study SNe Ia near maximum brightness in the ultraviolet (UV) wavelengths (Petrushevska et al. 2017) and with a time series to study optical spectral feature evolution (Johansson et al. 2021; Gall et al. 2024). gLSNe have also been proposed (Refsdal 1964; Goobar et al. 2002) as an independent way of measuring H_0 via time-delay distances, demonstrated with the observations of SN Refsdal (Kelly et al. 2023) and SN H0pe (Chen et al. 2024; Frye et al. 2024; Pascale et al. 2024; Pierel et al. 2024b). As SNe Ia play a central role both in the study of dark energy properties and galactic chemical enrichment, it is important to have a detailed view of the explosions at $z > 1$. At intermediate redshifts ($z \sim 0.5$), there have been studies comparing the spectroscopic properties, both the optical and the UV to low-z ($z < 0.1$) SNe (e.g. comparisons in Sullivan et al. 2009; Foley et al. 2012; Maguire et al. 2012). It is well known that the post-standardization SN Ia luminosity depends on the host galaxy properties (Hamuy et al. 1996; Sullivan et al. 2003, 2010; Kelly et al. 2010). Therefore, since the galaxy properties (mass, age, and metal and dust content) change with cosmic time, it is clearly important to quantify how the SN Ia properties differ with redshift. Hook et al. (2005) analysed a sample of 14 SNe Ia in the redshift range $0.17 \leq z \leq 0.83$, finding the spectroscopic time series and the Ca II H&K velocities to be indistinguishable from low-z SNe Ia. Using a large sample of SNe Ia from the Supernova Legacy Survey up to $z \sim 1$, Bronder et al. (2008) found no evolution in the rest-frame velocities and pseudo-equivalent widths (pEWs) of the SNe Ia. Sullivan et al. (2009) find – by comparing low-z spectra to the intermediate- and high-z SNe (Riess et al. 2007; Ellis et al. 2008) – that changes in the average spectroscopic properties are primarily attributed to the evolution in the SN Ia demographics with redshift. Accounting for the different stretch distributions across redshift, they do not find differences between the low- and high-z SNe Ia. Maguire et al. (2012) compared a sample of low-z near-UV spectra to the high-z sample from Ellis et al. (2008) and found a UV flux deficit in the distant SNe Ia at the $\sim 3\sigma$ level. Balland et al. (2009) found that $z > 0.5$ had shallower features of intermediate-mass elements compared to the $z < 0.5$ sample. Seen synoptically, the studies would suggest a small, potentially appreciable difference, but such an effect is far from certain. The studies present very high fidelity spectra but they are limited in the phase range (typically <10 d from maximum light) and are mostly at $z < 1$. It is, therefore, critical to study the spectroscopic properties of SNe Ia at larger lookback times. Most spectra of intermediate-redshift SNe Ia are also observed near maximum light, therefore, it is important to study the spectral energy distribution (SED) at different phases of the explosion.

Here, we study the post-maximum rest-frame optical spectrum of a lensed SN Ia, named SN Encore, at $z = 1.95$. SN Encore was discovered on 2023 November 17 by the *JWST* (*JWST*-GO-2345, PI: Newman). The discovery epoch includes spectroscopic and photometric observations, details of which are summarized in Pierel et al. (2024a). Remarkably, the host galaxy of SN Encore also hosted SN Requiem (Rodney et al. 2021), which was a photometrically classified SN Ia. The data for SN Encore allow us to compare the properties of SNe Ia at a lookback time of 10.5 Gyr, i.e. when the universe was around 3.3 Gyr old with the properties of SNe Ia at present day. The observations of SN Encore were obtained at ∼few rest-frame weeks after maximum. At these epochs, the ejecta temperature has decreased to ∼7000 K such that there is a recombination wave that leads to an ionization transition from doubly to singly ionized species of iron group elements (Kasen 2006; Blondin, Dessart & Hillier 2015). This manifests as a rebrightening in the redder filters, seen as a second maximum in the $izYJHK$ filters (e.g. Hamuy et al. 1996; Folatelli et al. 2010; Dhawan et al. 2015) and a shoulder in the Vr filters. The timing of this second peak can be used to measure the total amount of radioactive material in the ejecta (Kasen 2006; Dhawan et al. 2016). Along with intermediate-mass elements, e.g. Si, Mg, S, at these phases, the spectrum also has lines from iron group elements (Jack, Baron & Hauschildt 2015). Such spectroscopic studies are important to test what the explosion scenario and progenitor of an SN Ia is. While it has been known that SNe Ia arise from the thermonuclear explosion of a CO WD in a binary system (Livio & Mazzali 2018), the nature of the progenitor, e.g. the mass of the WD and the companion star, is poorly understood. Potential suggestions include sub-Chandrasekhar mass ($M_{\rm Ch}$) WD that detonates from a secondary supersonic shock triggered by a helium shell detonation (Woosley & Weaver 1994; Shen et al. 2021a). An alternate scenario is a sub-$M_{\rm Ch}$ double detonation of a hybrid He–CO WD (e.g. Perets et al. 2019; Pakmor et al. 2021, 2022; Roy et al. 2022). Comparing the model predictions to observations of high-z SNe Ia is an important route to understand the progenitor channels at earlier epochs in cosmic history. Such comparisons are possible due to suite of new photometric and spectroscopic instruments with the *JWST*, e.g. Near-Infrared Camera (NIRCam; Rieke, Kelly & Horner 2005) and Near-Infrared Spectrograph (NIRSpec; Jakobsen et al. 2022).

In this paper, we present and analyse spectroscopic observations of an SN Ia at $z \sim 2$ coinciding with the phases corresponding to the second maximum, some of the first at this phase and high-z (see also Pierel et al. 2024a). Therefore, we infer the spectroscopic properties of SN Encore and compare them to low- and intermediate-redshift spectra from the literature to test for any evolution of SN Ia properties with cosmic time. The data set is presented in Section 2 and results in Section 3. Results are discussed and conclusions are presented in Section 4.

2 DATA

SN Encore was discovered in the *F*150*W* NIRCam imaging taken 2023 November 17 (MJD 60265) by noticing a point source on top of a smooth galaxy distribution and then comparing the data with a *Hubble Space Telescope* Wide Field Camera 3/Infrared (WFC3/IR) *F*160*W* image taken on 2016 July 18, MJD 57587 (Newman et al.

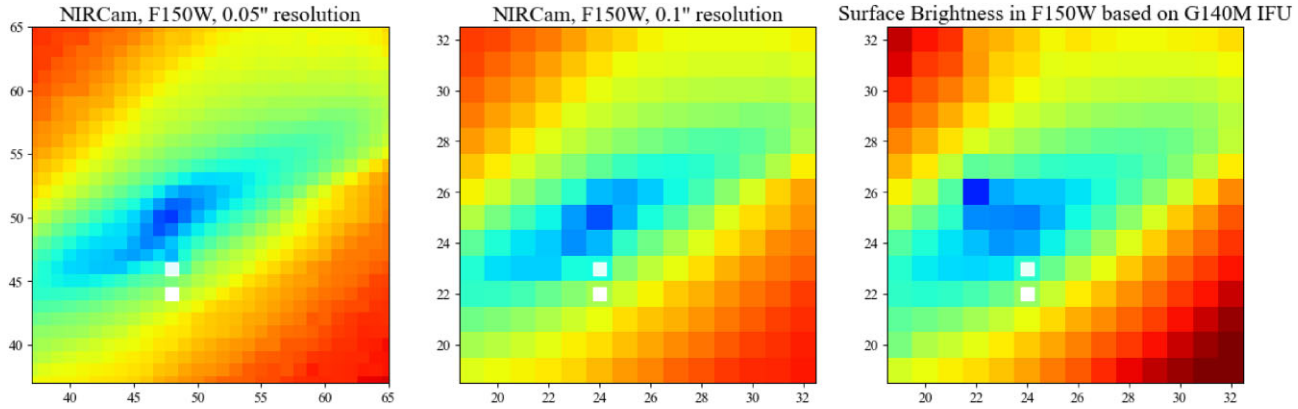

Figure 1. A summary of the NIRCam imaging and NIRSpec G140M IFU data obtained for SN Encore (corresponding to the brightest image, i.e. image A). Left: *F*150*W* surface brightness map calculated using NIRCam images with 0.05 arcsec resolution with a north-up orientation. Blue colour indicates brighter pixels. White dots indicate the SN positions covered by the spaxels selected from the IFU data cube. The SN is distinct in the image compared to surrounding pixels with lower surface brightness. Middle: NIRCam image with 0.1 arcsec resolution with the same orientation. We mark the pixels of potential SN location as dots. Right: *F*150*W* surface brightness map from the G140M IFU cube with the predicted SN location as a dot.

2018). The filters are well matched in wavelength and transmission and the source was brighter than 24 AB mag. However, the separation of the source from the nucleus of the host galaxy, MRG-M0138, is ∼0.1 arcsec, which is approximately the pixel scale of WFC3/IR. Forced photometry confirmed that there was an increase in flux corresponding to the apparent brightness of SN Encore between the *F*160*W* and *F*150*W* imaging. Two images of the SN, image A and image B, were clearly visible in the *F*150*W* data, while a third image, image C, was revealed after subtracting the host galaxy light (Pierel et al. 2024a). Lens model predictions suggest that the next image will arrive by the end of the decade, allowing a dedicated follow-up campaign similar to SN Refsdal (Kelly et al. 2016). The host galaxy of the SN, MRG-M0138, is red and passive, already suggesting that there is low star formation, and hence, that the SN is likely of Type Ia (Rodney et al. 2021).

The data used include *JWST* NIRCam images and NIRSpec integral field unit (IFU) spectroscopic observations, both from a Cycle 1 program (Program ID: 2345, PI: Andrew B. Newman). Observations of G235M were taken on 2023 November 17, and G140M data were taken on 2023 December 27. We used the following combination of grating and disperser: G140M/F100LP and G235M/F170LP, with total exposure times of 8228 and 7644 s, respectively. Exposures with the same integration time were also taken on a nearby background field. Data are processed by a modification of the *JWST* pipeline with version 1.13.4. Raw data were downloaded from the *Barbara A. Mikulski Archive for Space Telescopes* (*MAST*). For this work, we used the *F*150*W* NIRCam images. For NIRCam image reduction, the Calibration Reference Data System (CRDS) reference files were defined by `jwst_1230.pmap`. In stage 1, the snowball rejection was activated. In stage 2, we used the default parameters in the pipeline. In stage 3, the final output image was oriented to be north-up by customizing the `rotation` parameter in the resampling step, and the `crval` parameter was modified to specify the right ascension (RA) and declination (Dec.) of the reference pixel for alignment with observations made by different instruments. Two output images with different spatial resolutions, 0.05 and 0.1 arcsec pixel^{-1}, were generated. For NIRSpec IFU data, we processed G140M/F100LP and G235M/F170LP spectra. The CRDS reference files are defined by `jwst_1225.pmap`. Modifications included activating NSCLEAN and turning off the default background subtraction to post-process sky subtraction instead of using the default 1D sky subtraction. In the `cube_build` step of stage 3, the output was oriented to be north-up, and parameters `ra_center`, `dec_center` and `cube_pa` were specified.

The supernova (SN) is visible in the high-resolution (0.05 arcsec pixel^{-1}) NIRCam image (left panel of Fig. 1) but less distinct in the 0.1 arcsec pixel^{-1} NIRCam image (middle panel of Fig. 1) and NIRSpec IFU data (right panel of Fig. 1). We first aligned the spectra and images by specifying coordinate-related parameters and ensuring the rotation angle was consistent with north-up. Surface brightness maps were generated using filter *F*150*W*, and the IFU centre was adjusted to minimize the difference between the surface brightness map from the NIRCam image and the NIRSpec IFU G140M/F100LP cube. We performed pixel-to-pixel subtraction of background spectra from the target data cube after cleaning outliers from the background. The host galaxy properties for MRG-M0138 are described in Newman et al. (2018). We isolated the SN spectra by subtracting an estimated the host galaxy spectrum at the same surface brightness, using both the G140M and G235M gratings. The G140M grating enabled alignment with the *F*150*W* NIRCam image, revealing the SN's location. G235M spectroscopy was aligned with G140M using their overlapping wavelength ranges. SN spaxels showed unique spectral features distinct from the galaxy's spectra. As shown in Fig. 1, we selected two spaxels in the IFU data as the potential locations of the SN.

For the host galaxy subtraction, we established contour levels based on the *F*150*W* surface brightness map for the G140M data cube, which allowed us to extract the background galaxy's spectra from spaxels matching the surface brightness levels of the SN spaxels. Two spaxels for SN locations are marked as white dots in Fig. 1. Neighbouring pixels from the SN spaxels were masked when calculating the host galaxy spectra. The host spectra were calculated as the median spectrum of the host galaxy in the same value levels of the two SN spaxels, which include 20 and 46 spaxels for the two SN spaxels, respectively. Finally, the SN spectrum was isolated by subtracting the median spectrum of the background galaxy from the observed SN spaxels. The extracted spectra are shown in Fig. 2.

3 RESULTS

In this section, we infer the SN type and age of SN Encore spectroscopically. We infer the phase of the observations from different

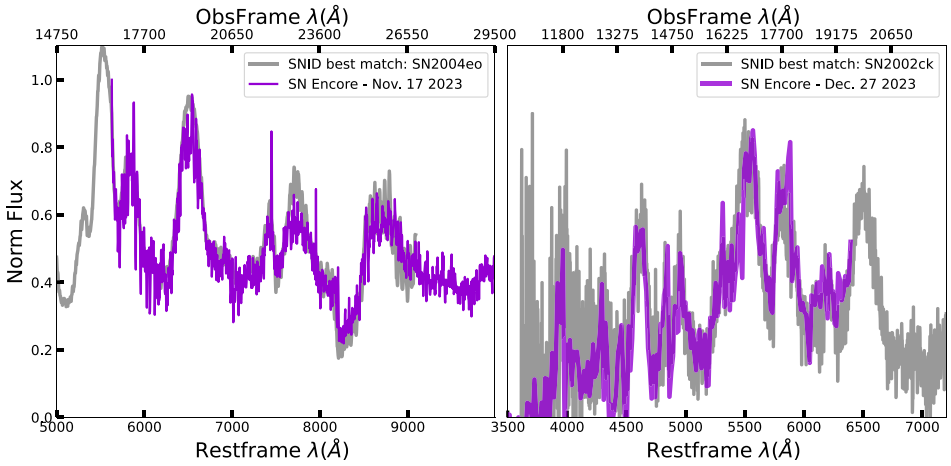

Figure 2. SNID fit to the spectrum taken on 2023 November 17 with the G235M grating and on 2023 December 28 with the G140M grating. They were fitted independently, both with the host redshift free and fixed (see text for details). For the first epoch, the top match is SN 2004eo at +29 d and 8 of the top 10 matches are 'Ia-norm'. For the second epoch, the best match is SN 2002ck, a normal SN Ia at +37 d, also with 8 out of the top 10 matches being normal SN Ia.

spectral matching procedures. First, we use the SN identification code SNID (Blondin & Tonry 2007) to simultaneously infer the SN type and age. Secondly, we use empirical spectral templates, namely, the HSIAO template (Hsiao et al. 2007) and the latest iteration of the Spectral Adaptive Light curve Template (SALT3; Kenworthy et al. 2021) to infer the spectral age. We then test for signatures of evolution with cosmic time, we compare the SN Encore spectrum to an ensemble spectrum from the local universe ($z < 0.1$) SNe Ia, corresponding to the phase range around the same time as the SN Encore spectra. We compare the SN Encore spectra to composite spectra of normal SNe Ia using the KAEPORA data base (Siebert et al. 2019), described in Section 3.2.

We also quantify the similarity by comparing the spectral line velocities from individual low-z SNe Ia with those of SN Encore.

3.1 Typing and age inference

We infer the type and age of the SN by fitting SNID to the observed spectrum. We infer the spectral properties in the first instance with no prior on the fit. We find the best fit to a normal Type Ia supernova (Ia-norm), with the best fit to SN 2004eo. 9 of the 10 top matches are to 'Ia-norm' SNe. We independently fit the second epoch to get the best SNID match. 8 of the top 10 matches for the spectrum taken on 2023 December 27 are also to SN Ia-norm with the best fit to SN 2002ck (Fig. 2).

The age inference is based on the top eight fits with rlap, a metric used by SNID to determine how correlated/similar the two SN spectra are, >5 and grade classified as 'good'. We take the median and standard deviation of the top eight fits (as demonstrated in Blondin et al. 2008) as the inferred phase and find that the spectrum suggests a phase of 27.9 ± 5.3 d. In the second instance, we fit with a prior on the redshift from the host galaxy. If we fix the redshift in the fit to that from the host galaxy spectrum, we get a consistent estimate for the phase of 29.0 ± 5.0 d. We use this estimate for the analysis from here onwards. For the second epoch, fitting independently of the first spectrum, the best estimate of the age using the same methods as for the first epoch is 37.4 ± 2.8 d. For this epoch, it is independent of the prior on the redshift from the host galaxy. Therefore, based on the spectroscopic information we conclude that SN Encore a normal SN Ia.

We use a complementary technique to measure the phase of the spectra, with empirical templates for the SED. Since there are few spectral templates, we compare the results from different model fits. The models are fitted using a Markov chain Monte Carlo (MCMC) with EMCEE (Foreman-Mackey et al. 2013) with 20 000 steps and 5000 samples for 'burn-in'. In the first case, we use the HSIAO template (Hsiao et al. 2007), which is built from a library of ∼600 spectra of ∼100 unique SNe Ia. Fitting this template to the first observed spectrum of SN Encore, we find a best matching phase of 24.7 ± 1.1 d. When using the latest SALT3 model (Kenworthy et al. 2021), which was developed from ∼1200 spectra of 380 distinct SNe Ia, we get a phase of $28.7^{+2.0}_{-1.5}$ d which is in agreement at the $\sim 1\sigma$ level. Similarly for the G140M spectrum, the HSIAO model indicates an age of $25.6^{+3.1}_{-4.5}$ d and SALT3 model indicates an age of $30.9^{+4.4}_{-9.1}$ d. All the methods yield consistent phase inference to within 2σ (Fig. 3). The difference between the phases inferred for both spectra is consistent with the difference in the dates of observation, accounting for time dilation.

3.2 Low-z spectral comparison

An important test of the evolution of SNe Ia with cosmic time is the comparison of spectra between low- and high-z SNe (e.g. Ellis et al. 2008; Petrushevska et al. 2017). We compare the SN Encore spectra to the local SN Ia sample using the relational data base KAEPORA (Siebert et al. 2019). We restrict the low-z sample to spectra between +17 and +45 d, which is the possible range of phases for SN Encore. KAEPORA contains a large data base of almost 5000 spectra of nearly 800 SNe Ia. The data are homogenized to account for the diverse signal-to-noise ratios, cleaned by removing residual sky lines, galaxy emission, and cosmic rays, and corrected for the host and Milky Way extinction as well as deredshifted to the rest frame of the SN. We make composite spectra from the data base to compare with SN Encore (Fig. 4). We begin by removing peculiar SNe Ia, which are defined as being similar to SN 2002cx, SN 2002es, or classified as Ia-CSM. We generate 500 bootstrap realizations from the composite spectra as described in Siebert et al. (2019). Composite spectra allow us to visualize differences between complex spectral feature shapes, which might not be possible with summary statistics, e.g. pEWs or line velocities. The low-z composite spectra are compared to the G140M and G235M spectrum of SN Encore in Fig. 4. There are no

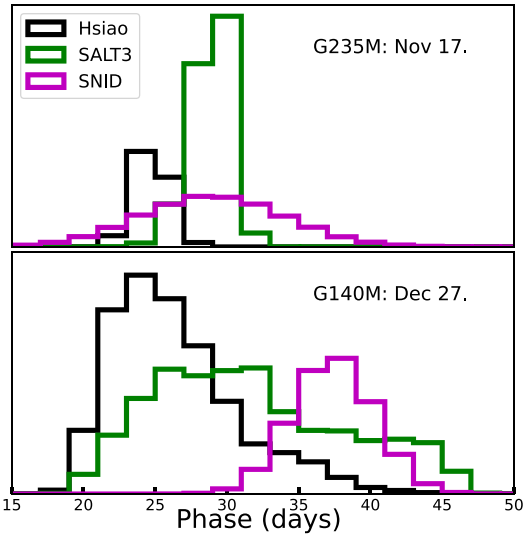

Figure 3. Posterior distribution of the inferred age for the G235M spectrum (top) and the G140M spectrum (bottom) for SN Encore using the three methods, i.e. HSIAO template (black), SALT3 (green), and SNID (magenta). The methods yield ages that are consistent with each other albeit with large errors.

obvious differences between the low-z spectra and SN Encore in this phase range. We also compare the SN Encore spectra to low-z spectra in $\Delta m_{15,\mathrm{B}}$ bins for values from 0.8 to 2.0. For comparison to the inference from the photometric data, we use an $x_1 = -1.39 \pm 0.13$ (Pierel et al., in preparation), where x_1 is the light-curve shape derived from the SED model used in cosmological inference, i.e. SALT3 (Kenworthy et al. 2021). The negative x_1 suggests that the SN is declining faster than the mean, while still being within the distribution expected for cosmological SNe Ia. Using the relation in Guy et al. (2007), this corresponds to a $\Delta m_{15,\mathrm{B}}$ of 1.34 ± 0.02. While we do not explicitly restrict either the comparison samples or models for our analysis, we use this inferred $\Delta m_{15,\mathrm{B}}$ as an indicative value. A comparison of the composite spectra in bins of $\Delta m_{15,\mathrm{B}}$ is shown in Fig. 5. We find that the composite spectra for the slowest declining SNe Ia are the least consistent with the observed spectra of SN Encore, while the other composite spectra agree very well. This is an independent test that SN Encore is a cosmological SN Ia with a faster-than-average decline rate.

SN Ia observing campaigns have also obtained high-fidelity spectra at intermediate- to high-z (e.g. Ellis et al. 2008; Balland et al. 2009, 2018). We note that while a comparison to composite spectra of intermediate-z SNe Ia would be very interesting, it is not viable since the spectra are observed close to maximum light, unlike the inferred phase of both the G140M and G235M spectra.

3.3 Spectral feature comparison

To quantify the spectroscopic comparisons further, we measure the spectral line velocity of the most ubiquitous features in an SN Ia, i.e. the Si II 6355 Å and the Ca II near-infrared (NIR) triplet. Spectral lines bluewards of the Si II 6355 Å feature cannot be measured very precisely with either spectrum, hence, we only analyse the two aforementioned features, observed in the G235M spectrum. The blue features are also difficult to measure without contamination at phases post-maximum (e.g. Folatelli et al. 2013, only measure it to ∼+20 d post-peak).

The spectra are fit with a Gaussian process (GP) smoothing using the tool SPEXTRACTOR[1] (see also Papadogiannakis 2019; Burrow et al. 2020). The spectral line velocities are inferred from Doppler shift between the wavelength minima λ_{m} computed by SPEXTRACTOR using the GP smoothing and the rest-frame wavelength of the feature (see Fig. 6 for the resulting fit).

Another metric used widely in the literature for spectral comparisons is the pEW. It is similar to the EW but since EWs require a continuum to be determined, which is not well defined for an SN Ia, a pseudo-continuum is defined, e.g. as a straight line fit between two local maxima (e.g. see Folatelli 2004). While pEWs are an important diagnostic of the explosion (e.g. Branch et al. 2006; Folatelli et al. 2013; Maguire et al. 2014), at high-z, we can expect a non-negligible contamination from the host galaxy (e.g. Foley et al. 2008). Therefore, to be conservative and use a 'cleaner' diagnostic, we only analyse the velocities of the two features.

For comparing to the low-z SNe Ia, we use measurements from the low-z as presented in Folatelli et al. (2013). This is a large, uniformly measured set of values that extend out to late phases, compatible with the phases of observation of SN Encore. The comparison to SN Encore is presented in Fig. 7. We find that both the line velocities of Si II 6355 Å and Ca II NIR are compatible with the distribution of value for the low-z sample showing no sign of evolution with redshift. We also compare the line velocity to other lensed SNe Ia, both at intermediate- ($0.1 < z < 0.5$) and high-z ($z > 1$). Spectra for SN H0pe are obtained from Chen et al. (2024) and the line width and velocity are measured with the same procedure as for SN Encore. We find no differences in the velocity evolution of either feature compared to the low-z sample for SN H0pe. For comparison we also plot the inferred line velocities for iPTF16geu, an intermediate-redshift lensed SN Ia at $z \sim 0.409$ (Goobar et al. 2017), with the line velocities as reported in Johansson et al. (2021), where the authors found that iPTF16geu showed a velocity evolution very similar to normal SNe Ia at low-z (see also Cano et al. 2018). Analysis of SN Zwicky (Goobar et al. 2023; Pierel 2023; Larison et al. 2024) an extremely compact lensed SN Ia will be presented in a forthcoming paper (Johansson et al. in preparation)

3.4 Comparison to explosion models

Spectra of SNe Ia at a few weeks post maximum contain important information regarding the elemental abundance and ionization state of the ejecta. At these phases, the IGEs in the ejecta transition from doubly to singly ionized, which is seen as a second maximum in the light curve at redder wavelengths (typically, i-band and redwards). This can be used as a diagnostic to distinguish between different model scenarios. In this section we compare the observations of SN Encore with synthetic spectra from different explosion scenarios. One of the open questions regarding SN Ia progenitors is the mass of the primary WD. Therefore, we compare the observations to both models for which the primary WD is Chandrasekhar mass ($M_{\mathrm{Ch}} \sim 1.4 M_{\odot}$, e.g. Khokhlov 1991) or significantly below it (sub-; e.g. Blondin et al. 2017). Here, we take a representative set of explosion models to cover the range of observables seen in the sample of 'normal' SN Ia, since SN Encore is a normal SN Ia. We briefly describe below the different scenarios considered in this work.

For the M_{ch} case, the leading model is the 'delayed-detonation' scenario (Khokhlov 1991; Seitenzahl et al. 2013). In this model, the explosion begins as a subsonic shock, or 'deflagration', which at

[1] https://github.com/astrobarn/spextractor

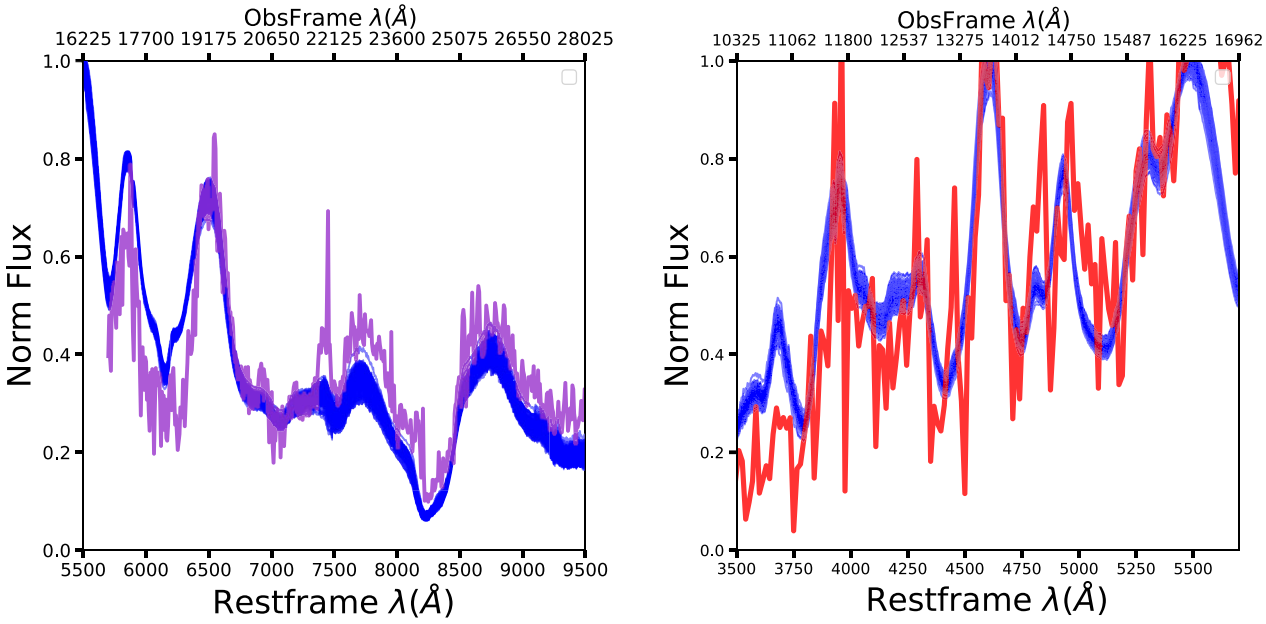

Figure 4. Left: Comparison of the mean optical spectrum from the KAEPORA data base in the phase range +17 to +45 d (blue) with the SN Encore spectrum taken on 2023 November 18 (violet). The spread in the mean spectrum is from the 500 bootstrap realizations of a composite spectrum from a total of 321 spectra in the phase range without telluric contamination. Since SN Encore is a 'Ia-norm' with a close to normal Δm_{15}, we restricted the range of comparison objects to $0.8 < \Delta m_{15} < 1.5$. Right: The same but for 2023 December 27 (red) compared to the composite spectrum from the SNe Ia between phase ranges +17 and +45 d.

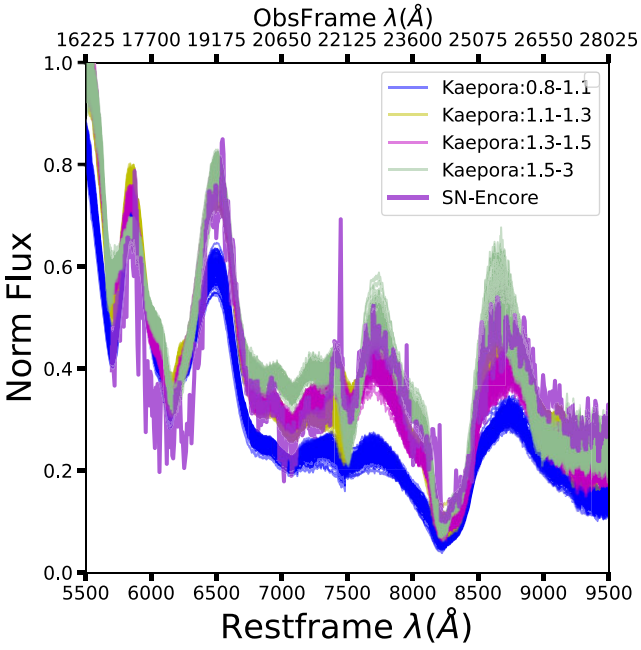

Figure 5. Comparison of the mean low-z SN Ia spectrum in the phase range permissible from the SNID inference, binned in Δm_{15}. All the composite spectra with a median $\Delta m_{15} > 1.1$ are consistent with the first observed spectrum of SN Encore.

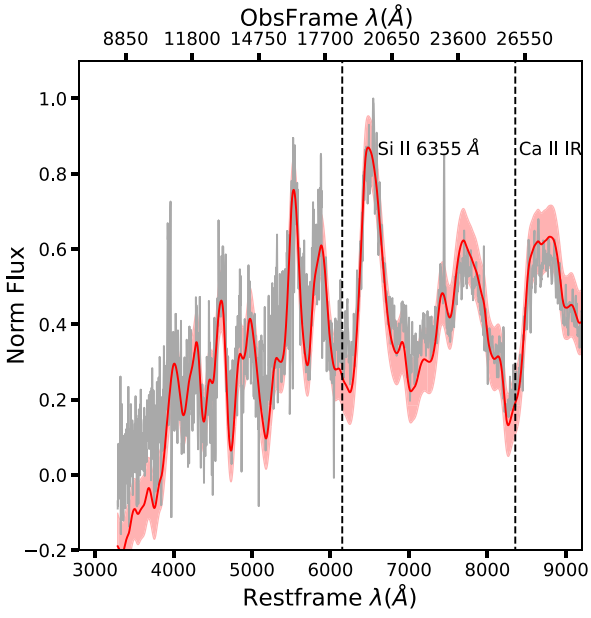

Figure 6. GP fit from SPEXTRACTOR (Papadogiannakis 2019) to the SN Encore spectrum (joined G140M and G235M).

a certain transition density, '$\rho_{\rm DDT}$', becomes a supersonic shock or a detonation. Without the pre-expansion or deflagration phase, the material of the WD would completely burn to iron-group elements (IGEs) without any intermediate-mass elements (IMEs), hence, the resulting explosion would not look like an SN Ia (Arnett 1969).

The subsonic shock pre-expands the WD reducing the density of the material, and this leads to the creation of both IGEs and IMEs giving rise to near-maximum light spectra that agree well with observations (Khokhlov 1991). The variation in the nucleosynthetic yields and, therefore, synthetic observables is determined by the transition density, $\rho_{\rm DDT}$. These models are referred to hereafter as DDC (Blondin et al. 2013). A variation of the $M_{\rm Ch}$ delayed-detonation models is the pulsational delayed detonations, which are

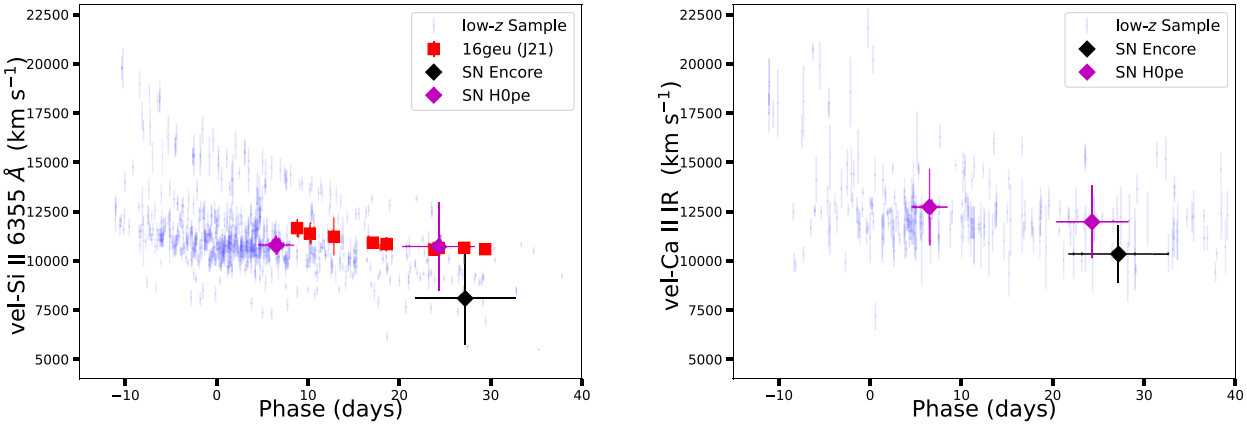

Figure 7. The evolution of the Si II 6355 Å (left) and Ca II NIR triplet line velocity (right) for low-z SNe Ia compared to lensed SNe Ia at high-z. The low-z sample is shown as smaller points. We find that the velocity of SN Encore is consistent with the low-z sample for the Si II 6355 Å.

very similar to the DDC models, except at early times wherein they have little mass at high velocity and hotter outer ejecta (hereafter PDDEL; Dessart et al. 2014).

For the sub-Chandrasekhar (sub-$M_{\rm Ch}$) models, the mass of the primary varies, which leads to differences in the elemental yields and the abundance of radioactive material (hereafter SCH). The models can explain a wide range of brightnesses and light-curve shapes, and there is observational evidence that faint SNe Ia arise from sub-$M_{\rm Ch}$ explosions (Blondin et al. 2017). While previously the models were disfavoured as the outer He shell (which was assumed to be very thick) produced Ti-group elements that predicted colours mismatched with observations (Woosley & Weaver 1994; Hoeflich et al. 1996), with recent thin shell models (e.g. Bildsten et al. 2007; Shen & Moore 2014), the agreement with observed spectra and colours is better (Pakmor et al. 2021, 2022; Shen et al. 2021a,b).

Recent studies have shown that the population of SNe Ia could comprise objects arising from either progenitor channel (see Blondin et al. 2017; Dhawan et al. 2018; Scalzo et al. 2019, amongst others). Therefore, we compare the synthetic observables from all the model categories describe above to the spectra of SN Encore. We investigate the radiative transfer from a wide range of explosion models, such that we can cover the known diversity of progenitor scenarios. Both the $M_{\rm Ch}$ (DDC and PDDEL) and sub-$M_{\rm ch}$ models span a range of ^{56}Ni masses, and in case of the SCH models, they also span a range of primary WD masses, since in this scenario the WD mass is the main determinant of the ^{56}Ni mass (e.g. Sim et al. 2010).

We pick the models in each class with $\Delta m_{15,\rm B}$ closest to the observations of SN Encore. For the scenarios tested, this corresponds to SCH3p5, DDC20, and PDDEL9 (in Fig. 8, the models are shown normalized to the flux around ∼6200 Å). We pick the model predictions closest to the phase of the G235M spectrum and find that all models can broadly reproduce the features in the G235M spectrum. Some of the most striking differences are in the region ∼9000 Å, which is likely a combination of strong Ca II, Fe II, and Co II lines (Blondin et al. 2015). While all models overpredict the relative flux in both these regions, the DDC models predict the brightest line ratio. However, the predicted strength of the line is sensitive to the phase inference, which has a few day uncertainty in our analysis. At blue wavelengths we see that the sub-Chandra models underpredict the flux at ∼6700 Å which could be due to differences in the Si II line strength. The DDC and PDDEL overpredict the flux at ∼5500 Å which is likely dominated by permitted transitions of Fe II and possibly forbidden [Co III], since the SN is transitioning to the nebular phase at such late epochs. If the true phase is not at

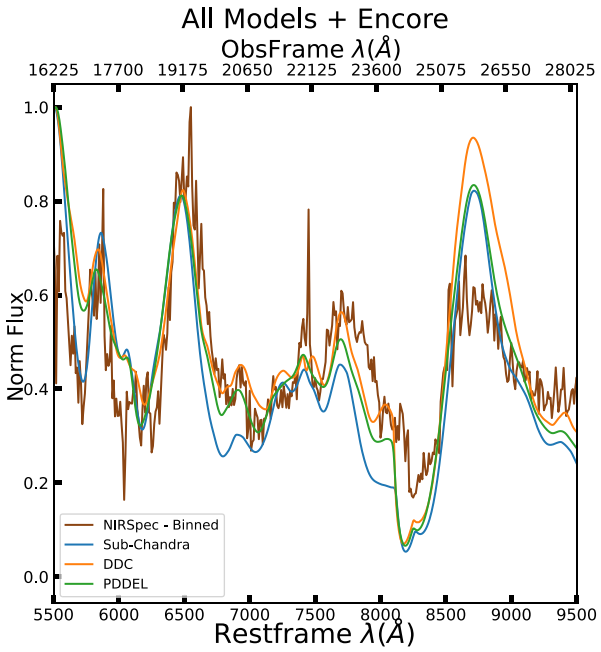

Figure 8. Comparison of the synthetic spectra for different explosion models with the observed spectrum of SN Encore within the estimated range based on both the photometry and the spectra.

the central value but within either the 68 or 95 per cent credible region, then the prediction from the DDC and PDDEL models matches the observed features better than the SCH model. Therefore, the inference regarding the model that most closely resembles the spectrum depends on having a precise, independent estimate of the epoch of the observation. Moreover, we note that this comparison is only performed for a single SN. In the future, such comparisons for a sample of high-z lensed SNe will be necessary to derive properties of the populations of SNe Ia, as done with composite UV spectra at $z \sim 0.5$ in Walker et al. (2012).

4 DISCUSSION AND CONCLUSION

We have analysed the spectra of SN Encore, a lensed SN Ia at $z = 1.95$ (Pierel et al. 2024a). Due to the boost in brightness from the lensing magnification, we can study a high-quality spectrum, a few

rest-frame weeks after maximum light, of an SN Ia with a lookback time of >10 Gyr. We find that the SN is consistent with a normal SN Ia subclassification from SNID template matching. The best-fitting phase of observations is 29.0 ± 5.0 d for the G235M spectrum and 37.4 ± 2.8 d for the G140M spectrum. This is consistent with the differences in observer frame days divided by $(1 + z)$ (see also White et al. 2024, for an analysis of time dilation with SN Ia light curves). We built a composite spectrum of low-z SNe Ia using the KAEPORA relational data base, we found no significant differences between the local sample and either of the SN Encore spectra. Binning the composite spectra based on the light-curve shape, we find that all except the slowest evolving subsample, i.e. with $0.8 < \Delta m_{15,B} < 1.1$ match the observed spectrum, which is consistent with the measurement of the shape of the light curve. We find no differences between the G140M observations of SN Encore and the mean low-z spectrum in the same wavelength region. In previous studies comparing the UV spectra of low- and intermediate-z ($z \sim 0.5$) SNe Ia, there has been evidence of depressed flux in the local SNe Ia compared to more distant SNe Ia in UV features at 2920 and ∼3180 Å. While our observations do not cover such blue features, future observations with G140M/F070LP will be critical to compare these features between local and very high-z ($z > 1$) gLSNe Ia.

As SNe Ia are precision probes of dark energy (DES Collaboration 2024), it is important to quantify systematics from any evolution of intrinsic properties with the age of the universe. The tests presented here show that based on post-maximum light spectra, there is no evidence of differences between the spectral properties of SN Encore and low-z SNe Ia. Complementary analysis of a lensed SN Ia at $z = 1.4$ – PS1-10afx (Quimby et al. 2014) – near-maximum light also demonstrated a similarity between the properties of low- and intermediate-z SNe Ia (Petrushevska et al. 2017). However, it was found that for PS1-10afx, the feature around 3500 Å is more prominent than the low-z sample. While there is not significant signal in that wavelength region for SN Encore, future observations will be critical to test whether such differences are also seen at later phases. We quantified the comparison by evaluating the spectral line velocities of SN Encore, as well as other lensed SNe Ia, namely, SN H0pe and iPTF16geu. We find that the line velocities measured for the intermediate- and high-z are consistent with the distribution observed for low-z SNe Ia.

With the advent of wide-field deep surveys of the transient sky, we expect to learn from current surveys (Sagués Carracedo et al. 2024; Townsend et al. 2024) and discover large samples of lensed SNe (Pierel & Rodney 2019; Arendse et al. 2024). Moreover, we can expect large samples of cluster-lensed SNe Ia to be discovered with *JWST* (Petrushevska et al. 2018). With a large sample of SN spectra, we can compare to predictions from different explosion models to infer what progenitor channels can explain the observed population of SNe Ia. Here, we illustrate this point by comparing to both M_{ch} and sub-M_{ch} models. The sub-M_{Ch} models underpredict the features near ∼6700 Å, whereas the DDC and PDDEL models overpredict the complex at ∼5500 Å , and the DDC models predict the strongest feature at ∼9000 Å. With future improvements in the model predictions we can use the spectra for a sample of SNe Ia to distinguish between different model scenarios. Strongly lensed SNe are, therefore, an excellent method to test cosmic evolution of SNe Ia both for controlling systematics in dark energy inference and understanding their progenitors.

ACKNOWLEDGEMENTS

Support for programs *JWST* GO-2345 and DD-6549 was provided by NASA through a grant from the Space Telescope Science Institute (STScI), which is operated by the Associations of Universities for Research in Astronomy, Inc., under NASA contract NAS5-26555. This paper is based on observations with the NASA/ESA *JWST* obtained from the *Mikulski Archive for Space Telescopes* at STScI. We thank Umut Burgaz for interesting discussions on spectral features. SD acknowledges support from a Kavli Fellowship and a Junior Research Fellowship at Lucy Cavendish College. JDRP was supported by NASA through an Einstein Fellowship grant no. HF2-51541.001 awarded by the STScI, which is operated by the Association of Universities for Research in Astronomy, Inc., for NASA, under contract NAS5-26555. CL acknowledges support from the National Science Foundation Graduate Research Fellowship Program under grant no. DGE-2233066. FP acknowledges support from the Spanish Ministerio de Ciencia, Innovación y Universidades (MICINN) under grant no. PID2022-141915NB-C21. This work was supported by research grants (VIL16599 and VIL54489) from Villum Fonden. RAW acknowledges support from NASA*JWST* Interdisciplinary Scientist grants NAG5-12460, NNX14AN10G, and 80NSSC18K0200 from GSFC.

DATA AVAILABILITY

Data are available via publically set repositories and web pages like WISEREP (Weizmann Interactive Supernova Data Repository).

REFERENCES

Arendse N. et al., 2024, MNRAS, 531, 3509
Arnett W. D., 1969, Ap&SS, 5, 180
Balland C. et al., 2009, A&A, 507, 85
Balland C. et al., 2018, A&A, 614, A134
Bildsten L., Shen K. J., Weinberg N. N., Nelemans G., 2007, ApJ, 662, L95
Blondin S. et al., 2008, ApJ, 682, 724
Blondin S., Dessart L., Hillier D. J., 2015, MNRAS, 448, 2766
Blondin S., Dessart L., Hillier D. J., Khokhlov A. M., 2013, MNRAS, 429, 2127
Blondin S., Dessart L., Hillier D. J., Khokhlov A. M., 2017, MNRAS, 470, 157
Blondin S., Tonry J. L., 2007, ApJ, 666, 1024
Branch D. et al., 2006, PASP, 118, 560
Bronder T. J. et al., 2008, A&A, 477, 717
Brout D. et al., 2022, ApJ, 938, 110
Burrow A. et al., 2020, ApJ, 901, 154
Cano Z., Selsing J., Hjorth J., de Ugarte Postigo A., Christensen L., Gall C., Kann D. A., 2018, MNRAS, 473, 4257
Chen W. et al., 2024, ApJ, 970, 102
Childress M. J. et al., 2015, MNRAS, 454, 3816
DES Collaboration, 2024, ApJ, 973, L14
DESI Collaboration, 2024, preprint (arXiv:2404.03002)
Dessart L., Blondin S., Hillier D. J., Khokhlov A., 2014, MNRAS, 441, 532
Dhawan S. et al., 2018, MNRAS, 480, 1445
Dhawan S., Leibundgut B., Spyromilio J., Blondin S., 2016, A&A, 588, A84
Dhawan S., Leibundgut B., Spyromilio J., Maguire K., 2015, MNRAS, 448, 1345
Ellis R. S. et al., 2008, ApJ, 674, 51
Flörs A. et al., 2020, MNRAS, 491, 2902
Folatelli G. et al., 2010, AJ, 139, 120
Folatelli G. et al., 2013, ApJ, 773, 53
Folatelli G., 2004, New Astron. Rev., 48, 623
Foley R. J. et al., 2008, ApJ, 684, 68
Foley R. J. et al., 2012, AJ, 143, 113
Foreman-Mackey D., Hogg D. W., Lang D., Goodman J., 2013, PASP, 125, 306
Frye B. L. et al., 2024, ApJ, 961, 171
Gall C. et al., 2024, ApJ, 972, 114
Ginolin M. et al., 2024a, preprint (arXiv:2405.20965)

Ginolin M. et al., 2024b, preprint (arXiv:2406.02072)
Goobar A. et al., 2017, Science, 356, 291
Goobar A. et al., 2023, Nat. Astron., 7, 1098
Goobar A., Mörtsell E., Amanullah R., Nugent P., 2002, A&A, 393, 25
Guy J. et al., 2007, A&A, 466, 11
Hamuy M., Phillips M. M., Suntzeff N. B., Schommer R. A., Maza J., Smith R. C., Lira P., Aviles R., 1996, AJ, 112, 2438
Hoeflich P., Khokhlov A., Wheeler J. C., Phillips M. M., Suntzeff N. B., Hamuy M., 1996, ApJ, 472, L81
Hook I. M. et al., 2005, AJ, 130, 2788
Hounsell R. et al., 2018, ApJ, 867, 23
Hsiao E. Y., Conley A., Howell D. A., Sullivan M., Pritchet C. J., Carlberg R. G., Nugent P. E., Phillips M. M., 2007, ApJ, 663, 1187
Jack D., Baron E., Hauschildt P. H., 2015, MNRAS, 449, 3581
Jakobsen P. et al., 2022, A&A, 661, A80
Jha S. W., Maguire K., Sullivan M., 2019, Nat. Astron., 3, 706
Johansson J. et al., 2021, MNRAS, 502, 510
Kasen D., 2006, ApJ, 649, 939
Kelly P. L. et al., 2016, ApJ, 819, L8
Kelly P. L. et al., 2023, Science, 380, abh1322
Kelly P. L., Hicken M., Burke D. L., Mandel K. S., Kirshner R. P., 2010, ApJ, 715, 743
Kenworthy W. D. et al., 2021, ApJ, 923, 265
Khokhlov A. M., 1991, A&A, 245, 114
Larison C. et al., 2024, preprint (arXiv:2409.17239)
Livio M., Mazzali P., 2018, Phys. Rep., 736, 1
Maguire K. et al., 2012, MNRAS, 426, 2359
Maguire K. et al., 2014, MNRAS, 444, 3258
Maguire K. et al., 2018, MNRAS, 477, 3567
Maguire K., 2017, in Alsabti A. W., Murdin P., eds, Handbook of Supernovae. Springer, Cham, Switzerland, p. 293
Newman A. B., Belli S., Ellis R. S., Patel S. G., 2018, ApJ, 862, 125
Pakmor R. et al., 2022, MNRAS, 517, 5260
Pakmor R., Zenati Y., Perets H. B., Toonen S., 2021, MNRAS, 503, 4734
Papadogiannakis S., 2019, PhD thesis, Stockholm University, Stockholm, Sweden
Pascale M. et al., 2024, preprint (arXiv:2403.18902)
Perets H. B., Zenati Y., Toonen S., Bobrick A., 2019, preprint (arXiv:1910.07532)
Perlmutter S. et al., 1999, ApJ, 517, 565
Petrushevska T., Amanullah R., Bulla M., Kromer M., Ferretti R., Goobar A., Papadogiannakis S., 2017, A&A, 603, A136
Petrushevska T., Okamura T., Kawamata R., Hangard L., Mahler G., Goobar A., 2018, Astron. Rep., 62, 917
Phillips M. M., 1993, ApJ, 413, L105
Pierel et al., 2023, ApJ, 948, 115
Pierel J. D. R. et al., 2024a, ApJ, 967, L37
Pierel J. D. R. et al., 2024b, ApJ, 967, 50
Pierel J. D. R., Rodney S., 2019, ApJ, 876, 107
Quimby R. M. et al., 2014, Science, 344, 396
Refsdal S., 1964, MNRAS, 128, 307
Rieke M. J., Kelly D., Horner S., 2005, in Heaney J. B., Burriesci L. G., eds, Proc. SPIE Conf. Ser. Vol. 5904, Cryogenic Optical Systems and Instruments XI. SPIE, Bellingham, p. 1
Riess A. G. et al., 1998, AJ, 116, 1009
Riess A. G. et al., 2007, ApJ, 659, 98
Riess A. G. et al., 2022, ApJ, 934, L7
Riess A. G., Livio M., 2006, ApJ, 648, 884
Rodney S. A., Brammer G. B., Pierel J. D. R., Richard J., Toft S., O'Connor K. F., Akhshik M., Whitaker K. E., 2021, Nat. Astron., 5, 1118
Roy N. C. et al., 2022, ApJ, 932, L24
Sagués Carracedo A. et al., 2024, preprint (arXiv:2406.00052)
Scalzo R. A. et al., 2019, MNRAS, 483, 628
Scalzo R. A., Ruiter A. J., Sim S. A., 2014, MNRAS, 445, 2535
Seitenzahl I. R. et al., 2013, MNRAS, 429, 1156
Shen K. J., Blondin S., Kasen D., Dessart L., Townsley D. M., Boos S., Hillier D. J., 2021a, ApJ, 909, L18
Shen K. J., Boos S. J., Townsley D. M., Kasen D., 2021b, ApJ, 922, 68
Shen K. J., Moore K., 2014, ApJ, 797, 46
Siebert M. R. et al., 2019, MNRAS, 486, 5785
Sim S. A., Röpke F. K., Hillebrandt W., Kromer M., Pakmor R., Fink M., Ruiter A. J., Seitenzahl I. R., 2010, ApJ, 714, L52
Sullivan M. et al., 2003, MNRAS, 340, 1057
Sullivan M. et al., 2010, MNRAS, 406, 782
Sullivan M., Ellis R. S., Howell D. A., Riess A., Nugent P. E., Gal-Yam A., 2009, ApJ, 693, L76
Townsend A. et al., 2024, preprint (arXiv:2405.18589)
Tripp R., 1998, A&A, 331, 815
Walker E. S., Hachinger S., Mazzali P. A., Ellis R. S., Sullivan M., Gal Yam A., Howell D. A., 2012, MNRAS, 427, 103
White R. M. T. et al., 2024, MNRAS, 533, 3365
Woosley S. E., Weaver T. A., 1994, ApJ, 423, 371
Zwicky F., 1937, Phys. Rev., 51, 290

This paper has been typeset from a TEX/LATEX file prepared by the author.